

Development of a sub-millimeter position-sensitive gas detector^{*}

DU Yan-Yan(都艳艳) XU Tong-Ye(徐统业) SHAO Ruo-Bin(邵弱宾)

ZHANG Deng-Feng(张登峰) HANAPIA Erlan ZHU Cheng-Guang(祝成光)¹⁾

MOE Key Laboratory for Particle Physics and Particle Irradiation, Shandong University, Ji'nan 250100, China

Abstract: Position-sensitive thin-gap gas detectors have been developed in the laboratory, based on the ATLAS Thin Gap Chamber. The signal collection structure has been redesigned while retaining other configurations to keep the good time performance of the detector. The position resolution was measured using cosmic muons for two versions of the detector and found to be 409 μm and 233 μm respectively. This paper presents the structure of these two detector prototypes, with the position resolution measurement method and results.

Key words: thin gap chamber, position resolution

PACS: 07.77.Ka, 29.40.Gx **DOI:** 10.1088/1674-1137/38/10/106001

1 Introduction

The Thin Gap Chamber (TGC) used in the ATLAS experiment [1] shows good performance in terms of its fast response and time resolution, but has limited position resolution. For future experiments, such as the ATLAS trigger system upgrade, it is desirable to improve the position resolution while retaining the timing performance. The main goal of the study described in this paper is to build a prototype detector based on the TGC, with a position resolution better than 300 μm and timing performance at least as good as the current TGC.

The TGC detector operates in saturated mode by using a highly quenching gas mixture of carbon dioxide and n-pentane, ratio 55%:45%. The TGC has many advantages, such as low sensitivity to mechanical deformations, small parallax, small Landau tails and good time resolution, but its position sensitivity is around 1 cm, determined by the geometrical width of the readout channel and the strength of the induced signal. To improve the position resolution, we concentrate on improving the signal readout method by fine tuning the structure of the detector.

Two versions of prototypes of the new detector, named the precision Thin Gap Chamber (pTGC), based on the ATLAS TGC, have been constructed and tested. We found the position resolution can be improved to be less than 300 μm , with the second version of the prototype, which meets the requirements.

In Section 2, the structure of the pTGC detector is described. Section 3 describes the position resolution

measurements for the pTGC. Finally, the results of the measurements are summarized in Section 4.

2 Construction of the pTGC

In developing the pTGC, two versions of the detector were constructed and tested, the first version being referred to as pTGC-I and the second as pTGC-II.

A schematic of the pTGC-I structure is shown in Fig. 1. It is similar to the structure of the ATLAS TGC, except that the positions of the strips for signal collection are modified. 48 copper strips of width 0.8 mm, with a spacing of 0.2 mm between strips, are etched on the inner surface of the 2 parallel PCB boards, which form a thin chamber. The anode wires, segmented at 1.8 mm intervals and perpendicular to the strip direction, are sandwiched in between the two PCB boards. The resulting size of the detector is defined by the number of wires and strips, which are 290 mm \times 50 mm.

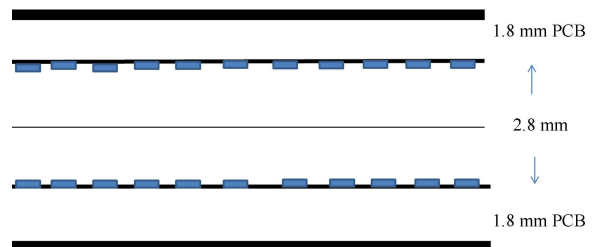


Fig. 1. Schematic structure of the pTGC-I chamber. The anode wires are placed in the middle of the chamber; copper strips are etched on the inner surface of the PCB board, perpendicular to the wire direction.

Received 4 November 2013, Revised 5 March 2014

^{*} Supported by NSFC (11075095) and Shandong Province Science Foundation (ZR2010AM015)

¹⁾ E-mail: zhucg@sdu.edu.cn

©2014 Chinese Physical Society and the Institute of High Energy Physics of the Chinese Academy of Sciences and the Institute of Modern Physics of the Chinese Academy of Sciences and IOP Publishing Ltd

While testing pTGC- I , it was found that electrical discharge between the wires and strips resulted in fatal damage to the frontend electronics, even though the design included a protection circuit between the detector and the frontend electronics board. This means that such a chamber would be unstable for a large detector and for a long time of running. Besides, the induced charge on the strips spread roughly from 5 to 6 mm, which leaves limited room for reducing the number of channels by enlarging the width of the strips. Therefore, based on pTGC- I , the pTGC- II was developed to deal with these problems.

The schematic of the pTGC- II structure is shown in Fig. 2. The strip width is enlarged to 3.8 mm (spaced at 0.2 mm intervals) with respect to pTGC- I , and a thin (100 μm) insulation layer is pasted onto the strip layer. The insulation layer is then coated with a thin ($\approx 30 \mu\text{m}$) graphite layer as the electrical ground to build the drift electrical field, together with the wires in high potential. This graphite layer protects the frontend electronics from discharge and can increase the spread size of the induced charge on the strip layer. We tune the surface resistivity of the graphite layer to be around 100 k Ω , taking the diffusion speed of the charge into consideration. The resulting size of the pTGC- II is 290 mm \times 200 mm.

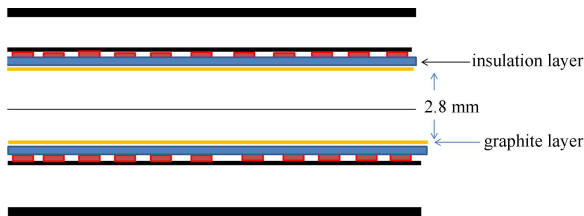


Fig. 2. Schematic structure of the pTGC- II chamber. Compared to pTGC- I , an additional insulation layer and graphite layer cover the etched copper strips.

Both detector prototypes used a gas mixture of carbon dioxide and n-pentane, ratio 55%:45%, as the working gas, and the anode wire voltage was set to 2900 V. These configurations are all the same as the ATLAS TGC detector, to keep the detector's good timing performance.

3 Position resolution measurement

To test the pTGC- I and pTGC- II detectors, three layers of identical chambers were placed in parallel with two layers of scintillator detectors to build a muon hodoscope (Fig. 3). Precisely machined spacers were inserted in between the detectors to fix the relative distance and to keep them parallel. To further reduce relative rotation between chambers, we used four long rigid screws to connect pre-designed positioning holes on the

detectors. From our measurements, we found the relative rotation effects to be smaller than the resolution of the detector.

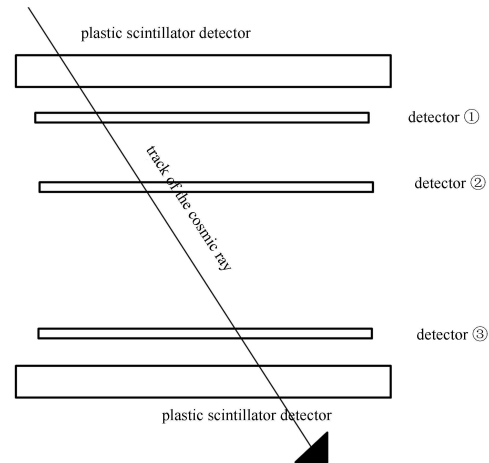


Fig. 3. The cosmic muon hodoscope used for the chamber testing. Plastic scintillator detectors are used for the trigger, and three identical pTGC chambers are placed in parallel between the two scintillator detectors.

The induced charge on each strip is integrated for the position calculation, based on the charge center-of-gravity algorithms. The measured hit positions on the three layers of chamber should form a straight line, due to the penetration power of muons. The deviation of the observed hit positions relative to a straight line is then used to calculate the position resolution of the detectors.

3.1 Signal definition

Using an oscilloscope, we first observed the induced signal in one wire group and three adjacent strips (limited by the number of channels on the oscilloscope), as shown in Fig. 4. It is apparent that the signals are clearly seen above the noise, and the signals on the strips are of different magnitudes, as expected.

For the position resolution measurement, we designed a much more complicated data acquisition (DAQ) system based on Gassiplex frontend electronics [2] to read out and digitize the induced charge from a number of channels of the three chambers in a more complex hodoscope [3]. Once the two scintillator detectors of the hodoscope are both fired, the DAQ is triggered. The trigger signal is sent to the detector front end electronics, which then close the gate to discharge the capacitor on which the signal charge has been integrated. The capacitor charges are then read out one by one, controlled by the clock distributed from the DAQ system. The charge is then digitized and saved to the computer.

The digitized charge, denoted by Q_i where i is the channel number, consists of three parts: electronic pedestal, noise, and charge induced by the muon hit.

First of all, we need to figure out the pedestal and noise for each channel. The method is to histogram the integrated charge for each channel using a soft trigger where no real muon-induced signal appears in the data. Fitting the histogram with a Gaussian function then gives the pedestal and the noise, denoted by P_i and σ_i respectively, as shown in Fig. 5, where the height of the histogram represents the pedestal and the error bar represents the noise of that channel.

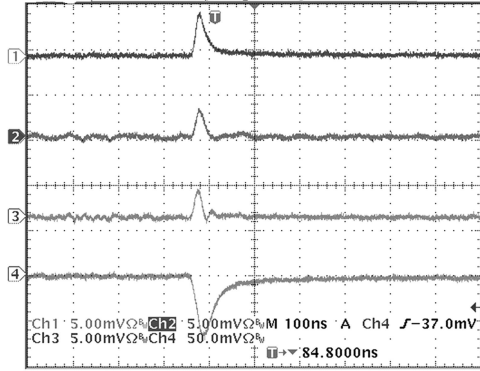


Fig. 4. The observed signals on the wires and several copper strips, induced by the same incident cosmic ray. The signal on the wire is negative, while the signals on the strips are positive.

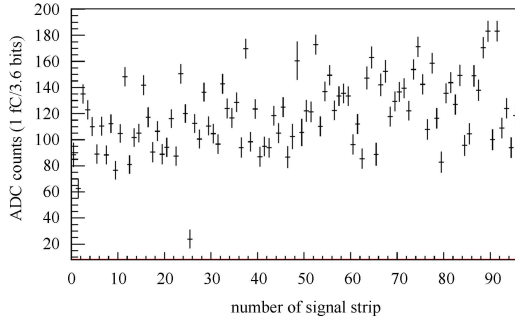


Fig. 5. Noise and pedestal distribution of 96 signal strips in one chamber (the x -axis is the signal strip number, the vertical coordinate is the pedestal value and the error bars represent the noise of that channel.)

In the analysis, if $Q_i > P_i + 3\sigma_i$, the channel is considered to be fired by a real muon hit, and the signal charge is calculated as:

$$S_i = Q_i - P_i. \quad (1)$$

The distribution of signal magnitudes of the largest signal in each cluster (cluster is defined in the next section), called the peak signal, is shown in Fig. 6. The distribution of signal magnitudes of the second largest signal in each cluster, called the second peak signal, is shown in Fig. 7. The distribution of the sums of all the charges in a single cluster is shown in Fig. 8. The correspondence between the magnitude of the signal and the charge is 1 fC/3.6 bits. We can then calculate that the

most probable charge of the peak signal in one cluster is 190 fC, and the most probable total charge of one cluster is 470 fC, which is consistent with the measurement given in Ref. [1].

3.2 Cluster definition

The charge induced by an incident muon is distributed over several adjacent strips, which are grouped in a “cluster”, used for the hit position calculation. For any given event, we search all the fired channels of one detector to group into clusters. To suppress fake signals from noise, if the cluster contains only one strip, it is dropped. The cluster size and number of clusters per detector per event are shown in Fig. 9 for pTGC-I and Fig. 10 for pTGC-II. It can be seen that in both cases, a single cluster contains an average of six strips, and almost all events consist of only one cluster, which

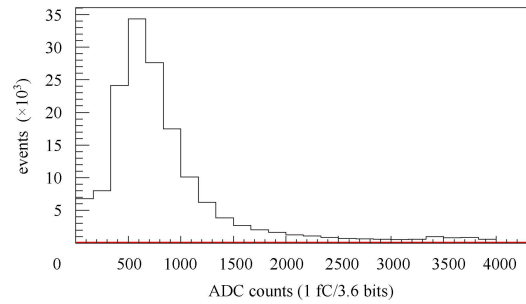


Fig. 6. Distribution of signal magnitudes of the peak signal in each cluster. The x -axis is the digitized charge collected.

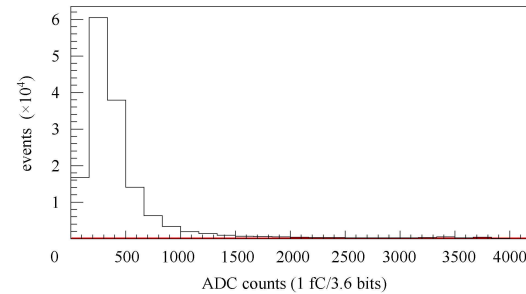


Fig. 7. Distribution of signal magnitudes of the second largest signal in each cluster.

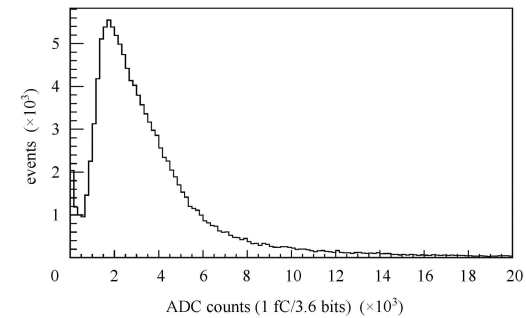


Fig. 8. Distribution of total charge induced in each cluster.

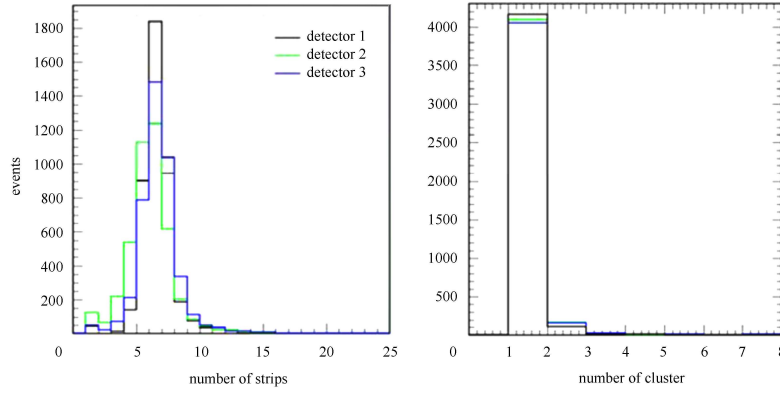


Fig. 9. (color online) For pTGC- I : (Left) Distribution of cluster sizes (number of strips in a single cluster). (Right) Number of clusters in a single chamber per triggered event.

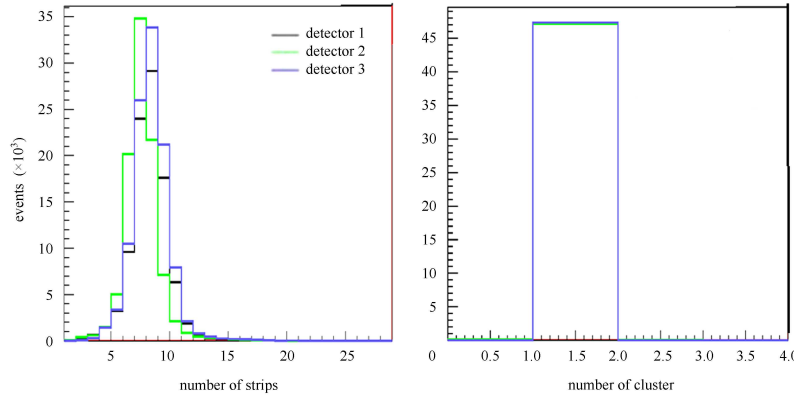


Fig. 10. (color online) For pTGC- II : (Left) Distribution of cluster size (number of strips in one cluster). (Right) Number of clusters in a single chamber per triggered event.

is consistent with our expectations. The hit position is then calculated for each cluster using the formula

$$x = \frac{\sum_i (S_i * x_i)}{\sum_i (S_i)}, \quad (2)$$

where x_i is the position of the centre of the i^{th} strip.

3.3 Position resolution

For safety in the design, the strips are etched on both inner surfaces of the PCB boards. A single event will then induce signals on both surfaces, giving double measurements of that hit, where the one with less problems is used in the later analysis. To compare the two measurements, denoted as x_1 and x'_1 , we fill $x_1 - x'_1$ into a histogram to check the broadness of the distribution. From a simple Gaussian function fit, we observe a narrow width of around $36 \mu\text{m}$, which means that the effect of electronic noise on the resolution is very small. This is consistent with our expectations from Fig. 5 and Fig. 6, where the signal magnitude is much higher than that of noise.

After the three hit positions x_1, x_2, x_3 are calculated for the three parallel chambers, to simplify the calculation, we first use x_1 and x_3 to calculate the expected hit

position on the second layer x_{2c} :

$$x_{2c} = x_1 \frac{L_{23}}{L_{12} + L_{23}} + x_3 \frac{L_{12}}{L_{12} + L_{23}}, \quad (3)$$

where L_{12} and L_{23} are the vertical distance between detectors 1, 2 and detectors 2, 3 respectively. Assuming the same position resolution σ for the three identical detectors, we know the resolution of x_{2c} , with error propagation, is:

$$\sigma_{2c} = \left(\sqrt{\frac{L_{23}^2}{(L_{12} + L_{23})^2} + \frac{L_{12}^2}{(L_{12} + L_{23})^2}} \right) \sigma \equiv k\sigma. \quad (4)$$

Filling $x_2 - x_{2c}$ into a histogram and then fitting with a Gaussian function, the width of the Gaussian is determined by the resolution of x_2 and x_{2c} :

$$w = \sqrt{\sigma^2 + (k\sigma)^2} = \sqrt{1 + k^2} \sigma. \quad (5)$$

We can then directly calculate the position resolution of the detector as

$$\sigma = \frac{w}{\sqrt{1 + k^2}}. \quad (6)$$

From Fig. 11 and Fig. 12, we obtain the position resolution as $409 \mu\text{m}$ for pTGC- I and $233 \mu\text{m}$ for pTGC- II.

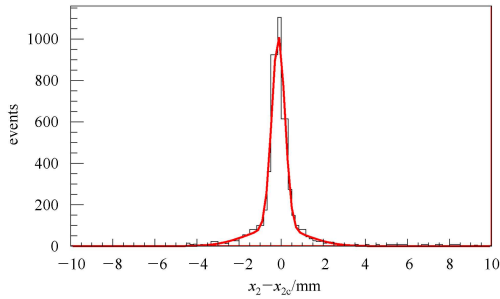


Fig. 11. The distribution of x_2-x_{2c} for pTGC-I. The corresponding position resolution of the chamber is $\sigma = \frac{w}{\sqrt{1+k^2}} = \frac{500 \mu\text{m}}{1.22} = 409 \mu\text{m}$.

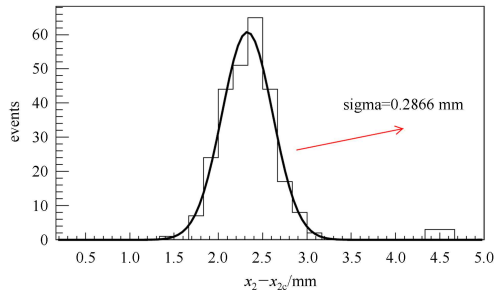


Fig. 12. The distribution of x_2-x_{2c} for pTGC-II. The corresponding position resolution of the chamber is $\sigma = \frac{w}{\sqrt{1+k^2}} = \frac{286 \mu\text{m}}{1.22} = 233 \mu\text{m}$.

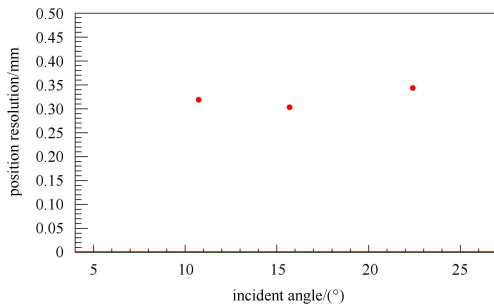


Fig. 13. The Gaussian width (defined in formula 5) relative to the cosmic ray incidence angle.

In tests, we see that the pTGC-II is more stable, with the protection of the extra graphite layer, and achieves a better resolution even with broader channels.

To look at the dependence of the detector position sensitivity on the incident angle of the muon, we divide the data into several groups. Each group of data contains events in which muons arrive with a specific incident angle. The analysis above was redone for each

group, and the result is shown in Fig. 13. It shows that the position resolution of pTGC-II is insensitive to the incident angle of muons.

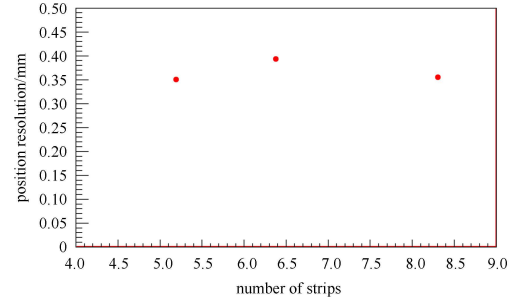


Fig. 14. The Gaussian width (defined in formula 5) relative to the number of strips per cluster used for position calculation. The x -axis is the number of strips per cluster used for position calculation.

To check the effect of electronic noise, we use subsets of the top highest signals in a single cluster to calculate the position resolution. The result is shown in Fig. 14, which shows that the resolutions are similar and that there is little effect from electronic noise.

4 Summary

Two pTGC prototypes, pTGC-I and pTGC-II, have been constructed and tested. With the basic structure and working gas unchanged from the original TGC, the new detector can attain the existing features of good time resolution and fast response, which are essential for triggering. The counting capability of the detector is affected by the speed of charge diffusion on the cathode plane. In the design of both prototypes, the cathode plane has a much lower resistance than the previous TGC, which will help to increase the counting capability.

By revising the signal collection structure and method, the position resolution is improved from the level of centimeters to be around $200 \mu\text{m}$ in the second version of the prototype, which also works stably for long runs. The measured worse resolution of the first version detector suffers from the much smaller signal spread and the less precise testing system. It should be noted that the resolution measured even for the second version detector is the global resolution of the detector, which includes the effects of detector non-uniformity over the whole sensitive area. This means that the measured resolution presented here is rather conservative and robust.

References

- 1 Aad G, Abbott B, Abdallah J et al. (Atlas collaboration). ATLAS Muon Spectrometer: Technical Design Report, 1997.
- 2 LIU Ming-Hui, YAN Zhen, ZHU Cheng-Guang et al. Nuclear Electronics and Detection Technology, 2008, 5: 949
- 3 XU Tong-Ye, DU Yan-Yan, WANG Xu et al. arXiv:1308.5751